Phys. Med. Biol. **44** (1999) 2765–2775. Printed in the UK PII: S0031-9155(99)03529-0

Design and construction of a ripple filter for a smoothed depth dose distribution in conformal particle therapy

Uli Weber and Gerhard Kraft

Gesellschaft für Schwerionenforschung, Biopysik, Planckstrasse 1, 64291 Darmstadt, Germany

Received 16 April 1999, in final form 6 August 1999

Abstract. The ripple filter was designed to broaden the Bragg maximum of carbon beams for the raster-scan technique, a special type of tumour-conformal ion beam treatment. In this technique the target volume is divided into individual layers that are treated sequentially by varying the energy from the accelerator stepwise. Because the unmodified Bragg maximum has a small half-width, below 1 mm for small energies (<160 MeV u^{-1}), homogeneous irradiation at small penetration depths of 2–6 cm can only be obtained by using a large number of energy steps. If the energy step is too large, ripples are produced in the superimposed depth dose distribution.

The ripple filter widens a Bragg peak to a Gaussian peak with a half-width of more than 2 mm. This helps to smooth the extended Bragg peak and to reduce the number of energy steps required by a factor of two to three, leading to significantly shorter overall irradiation times and a higher particle fluence per layer. The ripple filter consists of a 2 mm thick Plexiglass (PMMA) plate with a periodic structure of fine grooves. It can be mounted 60 cm upstream of the patient as a stationary device, because the fine structure of the grooves is completely washed out by the lateral scattering of the beam.

1. Introduction

Compared with conventional photon therapy, heavy-ion irradiation is characterized by an inverse dose profile, i.e. a low-dose plateau in the entrance channel and a sharp maximum (Bragg peak) near the end of the range. By varying the beam energy, the position of the Bragg peak in the tissue can precisely be adjusted in the beam direction. This makes heavy-ion beams a perfect tool for the treatment of deep-seated tumours (Tobias 1985, Kraft 1990).

At GSI Darmstadt a therapy unit has been constructed that realizes for the first time a three-dimensional target-conformal treatment based on active energy variation by the accelerator and lateral deflection by scanning the heavy ion beam with magnets (Goitein 1983, Haberer *et al* 1993, Badura *et al* 1998). For the irradiation the target volume is divided into individually shaped slices. Starting with the most distal one, for example, these slices are scanned one after the other, changing the accelerator energy from slice to slice. This technique allows tumour-conformal irradiation of almost any shape and an optimum biological efficiency inside and outside the tumour (Krämer and Jäkel 1997).

However, if the range steps from one slice to the next are wider than the width of the Bragg maximum, a periodic fluctuation (i.e. a ripple) is produced on top of the flat dose distribution (see figure 1, full curve). There are two approaches to solving this problem:

(a) One can increase the number of slices, leading to smaller range steps and a smoother depth dose profile. But for low energies and low penetration depths in particular the Bragg peaks are quite sharp (see figure 2, full curves), so that a large number of energy steps are

0031-9155/99/112765+11$30.00

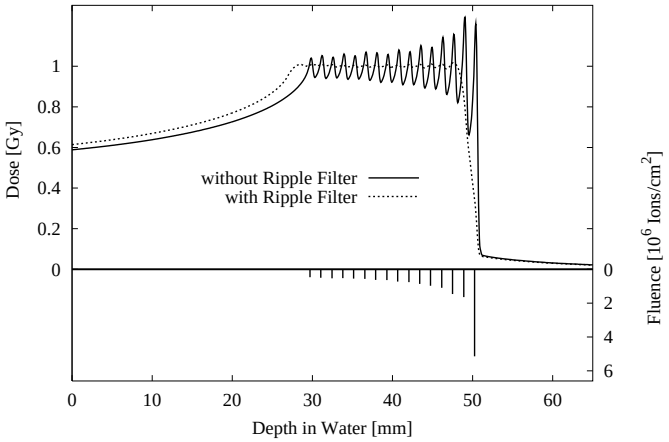

Figure 1. Comparison of an extended Bragg peak composed of 16 individual carbon Bragg curves with and without use of the ripple filter. The lower part shows the peak positions and the fluences of the superimposed Bragg curves.

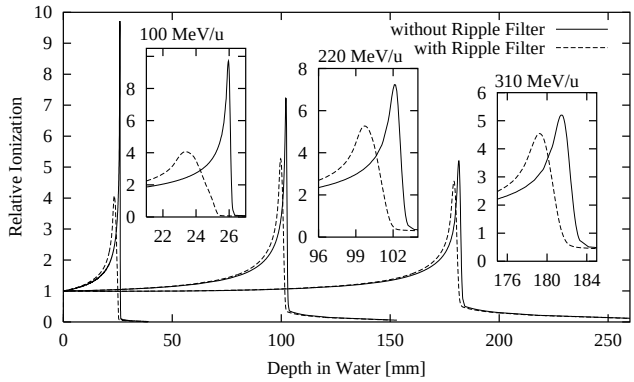

Figure 2. Comparison of individual carbon Bragg curves with and without a ripple filter at three different energies of 100, 220 and 310 MeV u^{-1} respectively. The broadening of the peaks connected with a shift to lower depth is clearly visible in the zoomed inserts.

required for a homogeneous dose distribution in the target volume. For instance a tumour at a depth between 2 and 5 cm would require more than 50 energy steps. This results in long irradiation times and difficulties in monitoring the beam currents and positions, because the particle fluence per energy step becomes low.

(b) The second and more favourable solution is to widen the Bragg peak using an additional energy spreading device.

In particle therapy performed up to now, the depth dose profile of the Bragg curve is greatly widened by passive devices like range-modulating propellers and ridge filters which produce an extended Bragg peak covering the whole depth of the tumour. Normally, those modulators are either rotated or moved very fast in order to mix the shifted peaks. On the other hand stationary ridge filters have been produced with narrow ridges (e.g. 1 cm), where the mixing takes place via the multiple scattering in the ridge filter itself. A synopsis of modulating devices and some relevant publications were compiled by Chu *et al* (1993). However, for a raster scan

system the requirements of an energy spreading system are different from that of the devices already described. Thanks to the energy variation of the beam, there is no need for a widening of the Bragg peak that covers the whole depth range of the target volume. Just a small peak widening is necessary in order to smooth the ripple of the superimposed depth dose profiles. Therefore, we have developed a so-called 'ripple filter', which is a stationary mini ridge filter that generates a small but exactly defined modulation effect.

2. Materials and methods

2.1. Production of a ripple filter

The ripple filter is made of a thin plate of Plexiglass (PMMA, 260 × 260 × 2 mm) and has a periodic structure of very fine and precisely cut grooves. They have to be manufactured to their desired form with a mechanical precision of about 5–10 μm. At a low speed (2–4 mm s^{-1}) a CNC machine cuts groove after groove into the Plexiglass using a fast rotating cutter (600–800 rpm). Continuous fluid cooling and fixing of the ripple filter on a vacuum table improves the cutting quality and the uniformity of the grooves. Figure 3 shows the design and the accurate groove structure of a 2 mm ripple filter used for heavy ion therapy at GSI. Optimization of the shape $t_p(x)$ of the grooves (i.e. the cutter) is described in section 2.3. However, a minimum thickness $t_{p,\min}$ of 0.3 mm is necessary for the stability of the Plexiglass plate.

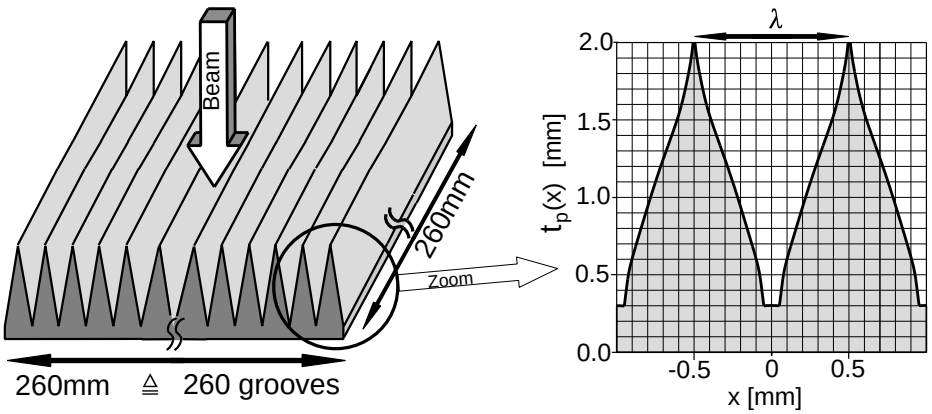

Figure 3. General layout of the ripple filter (left) and detailed design of the shape of the grooves defined by the function $t_p(x)$ which describes the thickness of the Plexiglass at a position x (right).

2.2. Bragg curve modulation by the ripple filter

The Bragg peak of a heavy ion beam passing perpendicularly through the ripple filter will be transformed by the grooves into a superposition of displaced Bragg curves. In practice, the typical beam diameter (4–10 mm) is far larger than the distance between the grooves (1 mm). The fraction of the beam that passes through the filter at a position x will be shifted by the water-equivalent thickness $t(x) = 1.165 t_p(x)$ in the z direction (see figure 3), using the density conversion factor 1.165 for PMMA to water (Jacob 1997). Provided that the lateral distribution of the beam intensity does not change within half a period λ of the groove structure, the depth

dose profile of the modulated Bragg curve b_{mod} in a water phantom is given by

$$b_{\mathrm{mod}}(z) = \frac{2}{\lambda}\int_0^{\lambda/2} b(z + t(x))\,\mathrm{d}x = \frac{2}{\lambda}\int_{t_{\min}}^{t_{\max}} b(z + t)X'(t)\,\mathrm{d}t \tag{1}$$

where $b(z)$ is the pristine Bragg curve. The periodic groove structure of the ripple filter is described by $t(x)$ or by its inverse $X(t)$. The derivative $X'(t)$ describes the transfer function of the ripple filter. For numerical computation of equation (1) we used Bragg curves measured with a step size of 50 μm in the Bragg peak region (see section 3.1). Calculating a quadratic spline interpolation of the measured points, a discrete form of the Bragg curves $b(z_i) = b(i\Delta z) = b_i$ with a very small step size of $\Delta z = 10\,\mu$m was obtained. The appropriate discrete form of equation (1) is

$$b_{\mathrm{mod},i} = \frac{2\Delta z}{\lambda}\sum_{j=j_{\min}}^{j_{\max}} b_{i+j}w_j \tag{2}$$

with $j_{\min} = t_{\min}/\Delta z$ and $j_{\max} = t_{\max}/\Delta z$. The weights $w_j = X'(j\Delta z)$ are discrete values of the transfer function $X'(t)$ with the same step size Δz used for the Bragg curves.

2.3. Optimization of the shape of the grooves

Gaussian Bragg peaks can be superimposed very smoothly and are therefore especially suitable for generating homogeneous depth dose profiles with a low ripple. This is numerically shown in appendix A. Therefore, the groove profile of the ripple filter has to be shaped in such a way that the resulting dose profile in the peak region is close to a Gaussian distribution. The ripple filter was primarily optimized for the very sharp 90 MeV u^{-1} ^{12}C Bragg peak (see figure 4, full curve), the lowest energy relevant for ion therapy. When the ripple filter modulates this peak to a Gaussian shape, a Gaussian shape will be produced for higher energies as well. This is due to the fact that the difference between the peak width of a 90 MeV u^{-1} beam and the peak width of a beam with higher energy is mainly induced by energy loss straggling, which follows a normal (Gaussian) distribution (Ahlen 1980). A convolution of two Gaussian distributions (one from the ripple filter and the other from the energy loss straggling) again results in a Gaussian distribution having a larger width.

The modified Bragg curve can only have a Gaussian form in the peak region. Therefore, the shape of the grooves (resp. the weights w_j) was calculated to produce an enlarged 90 MeV u^{-1} Bragg curve with a Gaussian shape in a depth range from 18.5 to 20.5 mm which determines the thickness of the ripple filter (2 mm). Using the method of least squares the weights w_j were optimized for a minimum difference χ^2 between $b_{\mathrm{mod},i}$ and the Gaussian function (see Gaussian curve in figure 4):

$$\chi^2 = \sum_{i=i_{\min}}^{i_{\max}}\left(\exp\left(\frac{-(i\Delta z - z_0)^2}{2\sigma^2}\right) - \sum_{j=j_{\min}}^{j_{\min}} b_{i+j}w_j\right)^2 \qquad w_j \geqslant 0 \tag{3}$$

with the parameters $\sigma = 1.0$ mm, $z_0 = 18.9$ mm, $i_{\min} = 18.5$ mm$/\Delta z$ and $i_{\max} = 20.5$ mm$/\Delta z$. After optimization the weights w_j were normalized so that $\Sigma w_j = 1$. As described in section 2.2, the weights w_j are discrete values of the derivative of the inverse of the desired function $t(x)$. Therefore the points (t_j, X_j) of the shape $t(x)$ $(0 < x < \lambda/2)$ can be calculated by integration (summation) of w_j:

$$t_j = j\Delta z, \quad X_j = \frac{\lambda}{2}\sum_{l=j_{\min}}^{j} w_l, \quad j = j_{\min}\ldots j_{\max}. \tag{4}$$

Including the conversion factor for Plexiglass the dataset $(1.165\,t_j, X_j)$ was directly used to manufacture the cutter (see section 2.1).

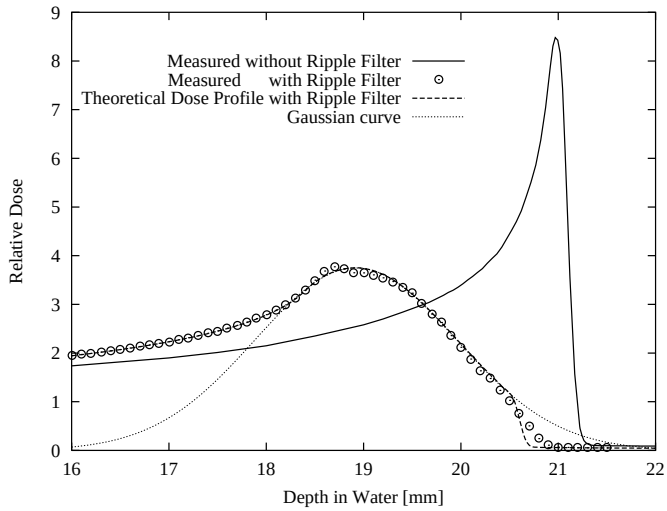

Figure 4. Measured Bragg peaks of a 90 MeV u^{-1} carbon beam with (circles) and without (full curve) use of the ripple filter. The broken curve represents the theoretical modulated Bragg curve from the optimization (see section 2.3). The dotted curve is the Gaussian curve ($\sigma = 1$ mm) that was aimed for in the optimization.

3. Results

3.1. Modulated Bragg curves

A direct result of the optimization of the values w_j is the theoretical shape of the modulated 90 MeV u^{-1} Bragg peak (equation (2)). This theoretical curve is shown in figure 4 (broken curve). In order to verify the optimization and the manufacturing process of the ripple filter we measured the modulated Bragg curve of a 90 MeV u^{-1} ^{12}C beam with the same experimental set-up (Schardt 1993) used previously for the measurement of the pristine Bragg peaks. These measurements have a resolution in depth of 50 μm and were repeated several times to improve the accuracy for the relative dose to 1–3%. Figure 4 shows the measured points of the pristine and the modulated Bragg curve, which agrees very well with the theoretical curve. Small differences at the maximum and at the end of the range are due to the fact that the peaks of the grooves could not be cut as sharply as desired. The mechanical realization has a peak width of about 60 μm where 30 μm is desired. However, the modulated peak has a nearly Gaussian shape in the desired depth range (see section 2.3).

Comparison of the measurements for the modulated and the pristine Bragg curves clearly determines experimental values of the weights w_j (equation (2)), which can be calculated with the help of a Fourier transformation. These weights agree quite well with the optimized weights, which before determined the form of the cutter. For treatment planning we use the experimental weights instead of the optimized weights. Because the weights w_j are always the same, regardless of the beam energy, it is possible to calculate the modulated Bragg curve for all relevant energies on the basis of the pristine Bragg curve by equation (2). Figure 2 shows the calculated effect of the ripple filter on ^{12}C Bragg curves for energies of 100, 220 and 310 MeV u^{-1} respectively. It demonstrates very well the increasing influence of the ripple filter with decreasing energy.

Actually, two types of ripple filter have been used for heavy ion therapy at GSI, one of thickness 2 mm which is described in this paper and a similar one with a thickness of 3 mm and groove distances of 1.5 mm for a stronger modulation effect.

3.2. The smoothing effect on extended Bragg peaks

The widening of the Bragg peaks to a Gaussian shape has a strong smoothing effect on an extended Bragg peak produced by active energy variation. The ripple filter works as a Gaussian filter and the inhomogeneity—or ripple—is wiped out, thus explaining why this device is called a ripple filter. This smoothing effect is best demonstrated in figure 1 (broken curve). The ripple filter reduces the required number of energy steps drastically by a factor of two to three or improves the homogeneity in the case of a given number of energy steps (see table 1). On the other hand it reduces the steepness of the distal fall-off (80–20%) from values between 0.2 and 2 mm (depending on the energy of the deepest Bragg curve) without a ripple filter to values between 1.3 and 2.2 mm with a ripple filter. However, this small loss of precision can easily be accepted.

Table 1. Calculated percentage amplitude (maximum deviation from the mean value) of the ripple on an extended carbon Bragg peak for different step sizes of the periodically superimposed Bragg curves. The maximum energy (deepest Bragg curve) and the step size determine the maximum ripple which always appears at the distal edge of an extended Bragg peak (see figure 1). The numbers in parentheses show the appropriate results with application of the ripple filter.

	Step size (mm)		
Max. energy (MeV u^{-1})	1.0	2.0	3.0
100	25 (2.0)	34 (3.8)	35 (14.0)
150	17 (1.5)	26 (2.6)	30 (12.0)
200	5.0 (0.9)	19 (1.5)	25 (9.5)
250	1.8 (0.5)	11 (0.9)	18 (6.5)
300	0.5 (0.3)	4.0 (0.7)	12 (4.0)
350	0.3 (0.2)	1.6 (0.5)	6.5 (1.5)

Using the ripple filter for treatment at GSI, the range steps of the scanned layers are set to 2 mm (3 mm for the ripple filter of 3 mm thickness) which guarantees a dose ripple always smaller than 4% and a very good target conformation with an acceptable number of slices.

3.3. Scattering effects

The ripple filter only works as a static device because multiple Coulomb scattering blurs the fine groove structure in the x-direction as demonstrated in figure 5. To avoid a transmission of the groove structure into the tissue, the beam having passed through the filter needs to have a sufficiently large angular distribution, and the distance d between ripple filter and patient has to be large enough. This can be expressed by the following condition:

$$\lambda \leqslant 1.6\, d\sigma_\alpha \tag{5}$$

where λ is the periodic distance of the grooves and σ_α is the width of the Gaussian angular distribution of the particle beam which is scattered by the exit window, the dose monitors and the ripple filter. This width can be calculated with sufficient precision according to the Molière formula for multiple Coulomb scattering (Gottschalk *et al* 1993). The particles passing through a point of the ripple filter yield a Gaussian spatial distribution within the distance d with a width

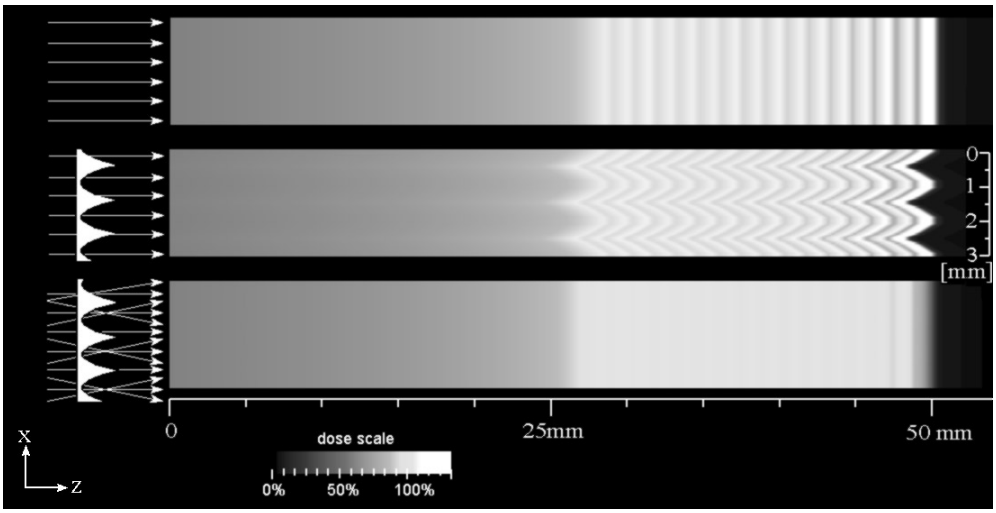

Figure 5. Calculated effect of blurring the structure of the ripple filter through multiple scattering: the upper stripe shows the two-dimensional dose distribution corresponding to figure 1 (full curve) without the ripple filter. The middle and the bottom ones show this dose distribution modulated by the ripple filter. The middle dose distribution was calculated without the scattering effect; therefore the structure of the grooves is transferred into the target volume. Adding on the inevitable multiple scattering the dose distribution becomes homogeneous (compare figure 1, broken curve).

of $\sigma_x = d\sigma_\alpha$. The factor 1.6 in equation (5) results from the fact that a periodic superposition of Gaussian curves is homogeneous ($\Delta < 0.1\%$) if their distances λ are less than 1.6σ (see appendix B).

The design of the ripple filter shown in figure 3 yields a homogeneous dose distribution for the following conditions:

- beam energy $E < 400$ MeV u^{-1} (^{12}C);
- the overall thickness of the scattering materials in front of the patient (e.g. exit window, detector system and air) is at least 150 mg cm^{-2};
- the distance between the ripple filter and the patient is approximately 65 cm.

These are typical parameters for a heavy ion therapy facility. For an irradiation unit with beam scanning, the beam width has no influence on the conditions listed. The only condition is that the scanning area should be much larger than the distance λ of the grooves.

The lateral beam width is slightly increased due to the scattering at the ripple filter (see table 2), but this side effect can be compensated for by the selection of a smaller beam diameter from the ion optics.

4. Conclusions

The ripple filter modifies the Bragg curve to a depth dose profile having a widened Gaussian peak. This offers significant advantages for irradiation with a scanning system using active energy stacking: the filter reduces the necessary number of energy steps and smooths the longitudinal dose distribution. This saves treatment time and increases the integral intensity per energy step and therefore the precision of the controlling detector system.

On the other hand the ripple filter shows no significant disadvantages because the beam quality with regard to the lateral beam profile is only slightly affected by the ripple filter and

Table 2. Effect of beam scattering at the ripple filter in dependence on the energy for a ^{12}C beam. The beam width (FWHM) in columns 2, 3 and 4 is always given at the patient position (65 cm behind the ripple filter). The second column contains the beam width w_0 without scattering at the ripple filter but with scattering at the exit window, air and the detectors. This width is mainly defined by the ion optics of the beam line and can be adjusted to suit the treatment. The third column shows the scattering effect for an infinitely thin parallel beam that is scattered (only) at the ripple filter. These values w_s are calculated with the Highland formula (Highland 1975) assuming an average thickness for the ripple filter of 120 mg cm^{-2}. The width of the beam scattered additionally at the ripple filter w_r (fourth column) can be calculated by the addition of columns 2 and 3 in quadrature: $w_r = (w_0^2 + w_s^2)^{1/2}$. Because of the quadratic addition of the scattering effect of the ripple filter, the total beam width increases only slightly through the ripple filter.

	FWHM of the beam (mm)		
Beam energy (MeV u^{-1})	Without ripple filter, w_0	Scattering effect, w_s	With ripple filter, w_r
100	8.0	2.4	8.4
150	6.0	1.6	6.2
	8.0	1.6	8.2
200	5.0	1.3	5.2
	8.0	1.3	8.1
250	5.0	1.0	5.1
	8.0	1.0	8.1
300	5.0	0.8	5.1
	8.0	0.8	8.0

the loss of steepness of the distal fall-off is in a tolerable range of 1 mm. The grooves of the ripple filter are so fine that the groove structure is blurred by the angular scattering. Therefore, the filter can be installed as a static device.

The ripple filter would be also beneficial for proton therapy. Considering the stronger scattering of protons, the distance of the grooves can be larger and therefore the grooves themselves could be deeper. This will result in a stronger modulation effect and could be useful for the treatment of small tumours (e.g. eye tumours) with proton beams because no further modulators such as linear or spiral ridge filters, are required.

Acknowledgments

The authors wish to thank Dr Dieter Schardt for his competent support during the experiments and Dieter Henke from the workshop of GSI for the excellent mechanical realization of the ripple filters.

Appendix A. Gaussian curve as a best function for a smooth periodic superposition

In order to determine the 'best' function $f(x)$ for a smooth superposition a criterion for smoothness has to be defined. Therefore, we calculate the integrated quadratic difference between 1 and the superposition of an infinite number of functions $f(x)$ displaced periodically by a distance λ:

$$\Delta(\lambda) = \frac{1}{\lambda}\int_0^{\lambda}\left(\sum_{i=-\infty}^{\infty}\lambda f(x - i\lambda) - 1\right)^2 \mathrm{d}x. \tag{6}$$

In practice equation (6) describes the (unidimensional) homogeneity of irradiation with a raster or a pixel scanning system when superimposing many dose profiles with a given function $f(x)$

in a transverse or longitudinal direction. The lower is $\Delta(\lambda)$ the better is the homogeneity of the superposition.

The optimization may be restricted to normalized functions which satisfy

$$\int_{-\infty}^{\infty} f(x)\,\mathrm{d}x = 1 \tag{7}$$

$$\int_{-\infty}^{\infty} f(x)x\,\mathrm{d}x = 0 \tag{8}$$

and

$$\sigma^2 = \int_{-\infty}^{\infty} f(x)x^2\,\mathrm{d}x = 1. \tag{9}$$

Since the beam intensity cannot be negative, another necessary restriction is that

$$f(x) \geqslant 0. \tag{10}$$

It is evident that many functions (e.g. the pulse square function) can be periodically superimposed yielding a constant function. But this is possible for one value of λ only. For other λ the homogeneity $\Delta(\lambda)$ is much worse. Therefore, the function $f(x)$ is searched, which achieves the best (lowest) mean homogeneity for a range of λ from σ to 2σ. This seems arbitrary, but superimposing dose profiles with a distance of σ up to 2σ is typical for the raster or pixel scan technique (Haberer *et al* 1993). In equation (11) we define the mean homogeneity H, which has to be minimized

$$H = \int_{\sigma}^{2\sigma} \Delta(\lambda)\,\mathrm{d}\lambda. \tag{11}$$

Unfortunately we could not find an analytical solution for this variational problem because the restrictions (7)–(10) make the problem too complicated. Therefore an iterative solution for a discrete-valued function $f(x_i)$ was found using an evolutionary Monte Carlo algorithm.

We start with a simple pulse square function that satisfies the conditions (7)–(10):

$$f(x) = \begin{cases} \dfrac{1}{2\sqrt{3}} & |x| < \sqrt{3} \\ 0 & \text{otherwise.} \end{cases} \tag{12}$$

For the Monte Carlo program a discrete form of $f(x)$ is used:

$$f_i = f(x_i) = f(i\Delta x) \qquad -N \leqslant i \leqslant N \tag{13}$$

with a fine step size $\Delta x = 0.05$ and a range $N\Delta x = 5\sigma$ (a smaller step size and a larger range do not change the result). For one iteration step we throw three random integer numbers l, m, n with $0 \leqslant l < m < n \leqslant N$ and a random value Δy_m in the interval $(-0.001, 0.001)$. Then six points of the discrete-valued function were changed

$$\begin{aligned} &f_l \longrightarrow f_l + \Delta y_l, \quad f_{-l} \longrightarrow f_{-l} + \Delta y_l \\ &f_m \longrightarrow f_m + \Delta y_m, \; f_{-m} \longrightarrow f_{-m} + \Delta y_m \\ &f_n \longrightarrow f_n + \Delta y_n, \quad f_{-n} \longrightarrow f_{-n} + \Delta y_n \end{aligned} \tag{14}$$

where

$$\begin{aligned} &\Delta y_m = \text{random value} \\ &\Delta y_l = \Delta y_m \left(\frac{n^2 - m^2}{l^2 - n^2} \right) \\ &\Delta y_n = -(\Delta y_m + \Delta y_l). \end{aligned} \tag{15}$$

The sense of this randomized change is that the function with the six new points again satisfies the restrictions (7)–(10).

Then we test with equation (11) whether H becomes smaller with the new values. If H becomes smaller and if the six new points are all positive, the next iteration step proceeds with the new values, otherwise with the old values.

After some 100 000 iteration steps this algorithm converges and the pulse function ($H \simeq 3 \times 10^{-2}$) has changed to a smooth function with a mean deviation from the normalized Gauss function that is smaller than 1% ($H \simeq 7 \times 10^{-6}$). This is what we wanted to show.

Appendix B. Homogeneity of a superposition of Gaussian functions

A periodic superposition $F(x)$ of normalized Gaussian curves with a period of λ can be written as follows:

$$F(x) = \sum_{i=-\infty}^{\infty} \frac{\lambda}{\sqrt{2\pi}\sigma} \exp\left(-\frac{(x - i\lambda)^2}{2\sigma^2}\right). \tag{16}$$

The mean value of $F(x)$ is equal to 1 and $F(x)$ oscillates around 1 with a period of λ. The amplitude of the oscillation depends on λ. The smaller λ, the lower the amplitude and the better the homogeneity of the superposition. The amplitude Δ can be set to $F(0) - 1$, because the superposition has its maximum values at the x-positions $\{\ldots, -\lambda, 0, \lambda, \ldots\}$. Table 3 shows the amplitudes for some values of λ/σ which are in a relevant range for raster scanning. If λ/σ is less than 1.6 a very smooth superposition with an inhomogeneity Δ of less than 0.1% is obtained.

Table 3. Amplitude of the oscillation (inhomogeneity) of a periodic superposition of Gaussian functions.

λ/σ	$\Delta = F(0) - 1$
1.0	$<10^{-8}$
1.4	8.5×10^{-5}
1.6	9.0×10^{-4}
1.8	4.5×10^{-3}
2.0	0.014
2.2	0.033
2.4	0.065
2.6	0.107

References

Ahlen S 1980 Theoretical and experimentical aspects of the energy loss of relativistic heavily ionizing particles *Rev. Mod. Phys.* **52** 121–73

Badura E *et al* 1998 First patient treated with carbon beams: status report of the heavy ion therapy at GSI *GSI Scientific Report 1997* GSI-98-1 (Darmstadt: GSI) pp 140–50

Chu W, Ludewigt B and Renner T 1993 Instrumentation for treatment of cancer using proton and light-ion beams *Rev. Sci. Instrum.* **64** 2055–122

Goitein M 1983 Beam scanning for heavy charged particle radiotherapy *Med. Phys.* **10** 831–40

Gottschalk B, Koehler A M, Schneider R J, Sisterson J M and Wagner M S 1993 Multiple coulomb scattering of 160 MeV Protons *Nucl. Instrum. Methods* B **74** 467–90

Haberer T 1994 Entwicklung eines magnetischen Strahlführungssystems zur tumorkonformen Strahlentherapie mit schweren geladenen Teilchen *PhD Thesis* Universität Heidelberg

Haberer T, Becher W, Schardt D and Kraft G 1993 Magnetic scanning system for heavy ion therapy *Nucl. Instrum. Methods* A **330** 296–314

Highland V L 1975 Some practical remarks on multiple scattering *Nucl. Instrum. Methods* **129** 497–9

Jacob C 1997 Reichweite CT-Zahl Beziehung von Phantommaterialien *PhD Thesis* Universität Heidelberg

Kraft G 1990 The radiobioloical and physical basis for radiotherapy with protons and heavier ions *Strahlenther. Onkol.* **166** 10–13

Krämer M and Jäkel O 1997 Therapy planning for heavy ion therapy *Advances in Hadrontherapy (Proc. Int. Week on Hadrontherapy ESI Archamps France (1995) and 2nd Int. Symp. on Hadrontherapy PSI and CERN Switzerland (1996))* ed U Amaldi, B Larsson and Y Lemoigne (Amsterdam: Elsevier) pp 351–8

Schardt D 1993 Bragg curve measurements with ionisation chambers *GSI Scientific Report 1992* GSI-93-1 (Darmstadt: GSI) p 336

Tobias C A 1985 The future of heavy ion science in biology and medicine *Radiat. Res.* **103** 1–33